



Originally published as:

Yue, X., Schreiner, W. S., Kuo, Y.-H., Hunt, D. C., Wang, W., Solomon, S. C., Burns, A. G., Bilitza, D., Liu, J. Y., Wan, W., Wickert, J. (2012): Global 3-D ionospheric electron density reanalysis based on multisource data assimilation. - Journal of Geophysical Research, 117, A09325

DOI: [10.1029/2012JA017968](https://doi.org/10.1029/2012JA017968)

Global 3-D ionospheric electron density reanalysis based on multisource data assimilation

Xinan Yue,¹ William S. Schreiner,¹ Ying-Hwa Kuo,¹ Douglas C. Hunt,¹ Wenbin Wang,² Stanley C. Solomon,² Alan G. Burns,² Dieter Bilitza,³ Jann-Yenq Liu,⁴ Weixing Wan,⁵ and Jens Wickert⁶

Received 18 May 2012; revised 21 August 2012; accepted 21 August 2012; published 29 September 2012.

[1] We report preliminary results of a global 3-D ionospheric electron density reanalysis demonstration study during 2002–2011 based on multisource data assimilation. The monthly global ionospheric electron density reanalysis has been done by assimilating the quiet days ionospheric data into a data assimilation model constructed using the International Reference Ionosphere (IRI) 2007 model and a Kalman filter technique. These data include global navigation satellite system (GNSS) observations of ionospheric total electron content (TEC) from ground-based stations, ionospheric radio occultations by CHAMP, GRACE, COSMIC, SAC-C, Metop-A, and the TerraSAR-X satellites, and Jason-1 and 2 altimeter TEC measurements. The output of the reanalysis are 3-D gridded ionospheric electron densities with temporal and spatial resolutions of 1 h in universal time, 5° in latitude, 10° in longitude, and ~30 km in altitude. The climatological features of the reanalysis results, such as solar activity dependence, seasonal variations, and the global morphology of the ionosphere, agree well with those in the empirical models and observations. The global electron content derived from the international GNSS service global ionospheric maps, the observed electron density profiles from the Poker Flat Incoherent Scatter Radar during 2007–2010, and f_oF_2 observed by the global ionosonde network during 2002–2011 are used to validate the reanalysis method. All comparisons show that the reanalysis have smaller deviations and biases than the IRI-2007 predictions. Especially after April 2006 when the six COSMIC satellites were launched, the reanalysis shows significant improvement over the IRI predictions. The obvious overestimation of the low-latitude ionospheric F region densities by the IRI model during the 23/24 solar minimum is corrected well by the reanalysis. The potential application and improvements of the reanalysis are also discussed.

Citation: Yue, X., et al. (2012), Global 3-D ionospheric electron density reanalysis based on multisource data assimilation, *J. Geophys. Res.*, 117, A09325, doi:10.1029/2012JA017968.

1. Introduction

[2] Global atmospheric, oceanic, and land fields reanalysis, which is carried out at the National Centers for Environmental Prediction (NCEP)/National Center for Atmospheric Research

(NCAR) and the European Centre for Medium-Range Weather Forecasts (ECMWF), has greatly impacted climate monitoring, scientific research, and numerical weather prediction (NWP) [Kalnay et al., 1996; Uppala et al., 2005]. Specifically, the reanalysis provides a gridded state representation of these fields by assimilating multisource observations into a physics-based model. Reanalyses of multidecadal series of past observations have become an important and widely utilized resource for the study of atmospheric and oceanic processes, climate, and predictability. However, this kind of reanalysis has not yet been extended to the upper thermosphere and ionosphere, which is the key region for radio wave propagation and low Earth orbiting (LEO) satellites. The main reason is probably the lack of sufficient, continuous, and global coverage observations of the ionosphere. The quantity, quality, and geographical coverage of ionospheric measurements have all significantly increased in the past decade. This increase is due to a wide range of ground- and space-based observations. Important ground-based networks include ionosondes, global

¹COSMIC Program Office, University Corporation for Atmospheric Research, Boulder, Colorado, USA.

²High Altitude Observatory, National Center for Atmospheric Research, Boulder, Colorado, USA.

³School of Physics, Astronomy, and Computational Science, George Mason University, Fairfax, Virginia, USA.

⁴National Space Organization, Hsinchu, Taiwan.

⁵Beijing National Observatory of Space Environment, Institute of Geology and Geophysics, Chinese Academy of Sciences, Beijing, China.

⁶GeoForschungsZentrum Potsdam, Potsdam, Germany.

Corresponding author: X. Yue, COSMIC Program Office, University Corporation for Atmospheric Research, 3300 Mitchell Ln., Boulder, CO 80301, USA. (xinanyue@ucar.edu)

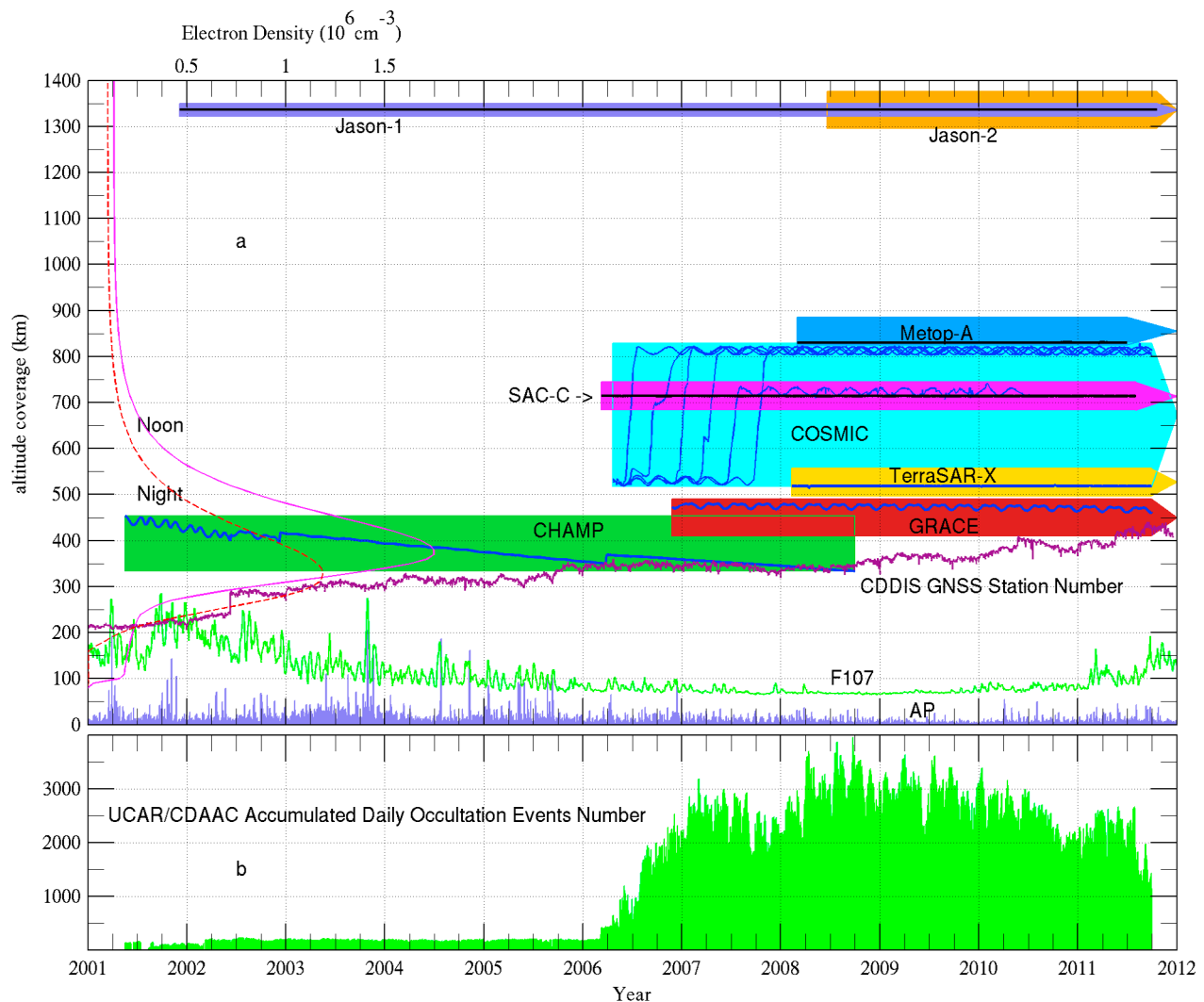


Figure 1. (a) Year and orbit altitude coverages of Jason-1/2 satellites and UCAR/CDAAC processed multiple radio occultation missions including CHAMP, GRACE, TerraSAR-X, COSMIC, SAC-C, and Metop-A. The solid line in each shadow is the corresponding daily average orbit altitude derived from the corresponding POD GPS observations. Also shown are F107 (green solid line) and daily AP (blue bar) indexes, the number of the available daily ground-based GNSS stations at the CDDIS IGS archive center (purple solid line), and the typical IRI2007 electron density profiles at local noon (magenta solid line) and midnight (red dashed line) over the equator under the moderate solar activity ($F107 = 150$) condition. The vertical axis unit is kilometers for the orbit altitude, and $10^{-22} \text{ W m}^{-2} \text{ Hz}^{-1}$ for F10.7 index, and AP is dimensionless. (b) The total number of daily radio occultation events accumulated at the UCAR/CDAAC.

navigation satellite system (GNSS) receivers, and incoherent scatter radars (ISR). But ground-based observations cannot be made over the oceans and have limited coverage in the polar regions. Many LEO satellites have been launched since the 1960s to measure the ionospheric in situ plasma density, temperature, and velocity. However, even the combined ground and LEO based observations are still far less than sufficient to estimate the global 3-D ionospheric states at a particular time.

[3] Since the success of the Global Positioning System/Meteorology (GPS/MET) experiment aboard the MicroLab 1 satellite in 1994, LEO based radio occultation (RO) has become an important and robust ionospheric sounding

technique [Anthes, 2011]. After that, many satellite missions, as shown in Figure 1, were successfully launched with RO payloads, accumulating a large number of RO data. The most significant and recent contributor to the RO data set is the well-known Formosa Satellite Mission 3/Constellation Observing System for Meteorology, Ionosphere and Climate (FORMOSAT-3/COSMIC, hereafter COSMIC for short) [Rocken *et al.*, 2000]. RO data has the advantage of limb sounding geometry, high accuracy, high vertical resolution, full global coverage, and no satellite dependent bias from the perspective of the ionosphere [Anthes, 2011]. Currently, at the COSMIC Data Analysis and Archive Center (CDAAC) of the University Corporation for Atmospheric Research

(UCAR), we are processing and archiving most of the RO missions' data as shown in Figure 1 [Schreiner et al., 2011]. Some of them are even processed in near real-time. These numerous RO slant measurements of total electron content (TEC) along the GNSS raypath offer us the first opportunity to do a global 3-D ionospheric electron density reanalysis similar to the NCAR/NCEP and ECMWF atmospheric fields reanalysis in the lower atmosphere, especially with the COSMIC data [Kalnay et al., 1996; Uppala et al., 2005; Yue et al., 2011b].

[4] The spatial and temporal evolution of the ionosphere, especially the electron density, has a significant impact on the radio signal propagation. Electron distribution in the ionosphere is determined by a number of processes, including ionization by solar EUV radiation and particle precipitation, chemical reactions including charge exchange and reactions with the neutral gas, transport by neutral winds and ion drifts, and ambipolar diffusion. Imaging the ionospheric electron density is important for both applications and scientific research (see the examples given by Bust and Mitchell [2008]). Many computerized ionospheric tomography (CIT) techniques have been developed in the past 2 decades since the pioneer work of Fremouw et al. [1992] and Austen et al. [1988]. The most frequently used CIT techniques were the algebraic reconstruction technique (ART) and the multiplicative ART (MART) [Andreeva, 1990; Raymund et al., 1990]. Early imaging work was mainly undertaken using LEO satellites beacon TEC measurements that provided 2-D regional studies [Pryse and Kersley, 1992]. With the availability of LEO-based GNSS observations, 3-D ionospheric electron density imaging using both ground-based and LEO-based slant TEC data was proposed [Hajj et al., 1994; Howe et al., 1998].

[5] In the past decade, data assimilation techniques, which have been successfully implemented in meteorological and oceanography studies, were introduced into the ionospheric research and application [Bust et al., 2004; Schunk et al., 2004; Wang et al., 2004; Yue et al., 2007a]. Schunk et al. [2004] at the Utah State University developed a Global Assimilation of Ionospheric Measurements (USU-GAIM) model based on a theoretical model and a Kalman filter. A team from the University of Southern California (USC) and the Jet Propulsion Laboratory (JPL) constructed a Global Assimilative Ionospheric Model (USC/JPL GAIM) using a different first-principles ionospheric model as the background model and a four-dimensional variational and Kalman filter optimization methods [Wang et al., 2004]. Bust et al. [2004] built the Ionospheric Data Assimilation Three-Dimensional (IDA3D) model using a three-dimensional variational data assimilation technique (3DVAR), which allowed ionospheric electron density to be imaged with respect to both space and time (4-D), by assimilating multisource observations into the background model. These data assimilation models have contributed significantly to the accurate ionospheric modeling, nowcasting, and even short-term forecasting.

[6] In this paper, we will describe and present some preliminary results of the global ionospheric electron density reanalysis based on a global ionospheric data assimilation model and the multisource data collected and processed at the UCAR/CDAAC. This research has the following purposes and significance.

[7] 1. UCAR CDAAC now is processing and archiving multiple RO missions data [Schreiner et al., 2011]. One of the ionosphere-related data products is the slant TEC along

the GNSS raypath from either the precise orbit determination (POD) antenna or the occultation antenna of these LEO satellites [Yue et al., 2011b]. A large number of RO slant TEC data have been accumulated over the past decade at UCAR. However, these arbitrary direction slant TECs are hard to use directly in scientific research and applications because of the localization problem. The LEO-based slant TEC, especially the occultation TEC, is expected to play a significant role in ionospheric imaging because it has a much higher vertical resolution than the ground-based observations [Bust and Mitchell, 2008]. The reanalysis will make full use of these data by combining them together with other available data sets and generating a global gridded 3-D electron density.

[8] 2. In most of the neutral atmosphere RO data retrieval methods, the ionospheric effect is treated without considering ionospheric variability [Syndergaard, 2000]. These methods can eliminate most ionospheric effects most of the time. However, this technique may not be accurate enough during daytime, solar maximum, or geomagnetic storm conditions, because of ray separation and large-scale ionospheric residuals [Mannucci et al., 2011; Syndergaard, 2000]. Ionospheric effects could be better calibrated by ray tracing based on a real 3-D, global ionospheric electron density field. This is especially important for atmospheric climate studies.

[9] 3. Ionospheric reanalysis can organize and archive past multisource observations in a more efficient way. It can be expected to benefit both scientific research and applications similar to the NCEP/NCAR and ECMWF reanalysis that was done for the research and application community in the lower atmosphere. Gridded electron densities can be used in ionospheric climate and weather research, such as solar activity and seasonal variations, ionospheric responses to geomagnetic storms and flares, and long-term trend analysis of the ionosphere [Yue et al., 2006]. Gridded h_mF_2 , N_mF_2 , and the global ionospheric map (GIM) derived from the reanalysis is particularly useful over the regions with relatively few or no ground-based observations.

[10] In this paper, we will assimilate various ionospheric observations into the IRI2007 model using a Kalman filter without time forwarding of error covariance in a 1 h time resolution monthly basis for only quiet days globally. The rest of the paper is organized as follows. The data sources, processing and error estimation are given in section 2. The global data assimilation model used in the reanalysis is described in section 3. Sections 4 and 5 show preliminary results and validations. Discussions and conclusions are given in sections 6 and 7, respectively.

2. Data Description

[11] The data that was used in the reanalysis included the slant TEC from global ground-based GNSS observations [Noll, 2010], the nadir vertical TEC over the ocean region observed by the altimeters on board Jason-1 and Ocean Surface Topography Mission (OSTM)/Jason-2 satellites [Dumont et al., 2009], and the slant TEC from multiple RO missions processed at the UCAR/CDAAC [Schreiner et al., 2011; Yue et al., 2011b]. The slant TEC obtained from RO satellites is composed of both the satellite overhead TEC (elevation $>0^\circ$) and the occultation TEC (elevation $<0^\circ$). The overhead slant TEC is usually observed by the POD antenna and can cover the ionosphere and plasmasphere above the

satellite orbit altitude [Yue *et al.*, 2011b]. The occultation TEC can be made by either the POD or the occultation antenna, depending on the satellite design. It can cover the whole ionosphere and plasmasphere up to the GNSS satellites altitude. The altitude of the tangent points of one occultation's GNSS ray varies from the Earth's surface to the LEO orbit altitude with very high vertical resolution (~ 1 Hz sampling rate corresponds to ~ 2 km). All RO satellites' occultation antennas are designed to begin sampling at a certain altitude (tangent point of GNSS ray) of the ionosphere (~ 80 km for Metop-A, ~ 400 and ~ 500 km for CHAMP and GRACE, and ~ 130 km for all others).

[12] The differential code bias (DCB) of most occultation antennas (except CHAMP) is difficult to calibrate [Yue *et al.*, 2011b]. For those missions which have no occultation observations from the POD antenna, the relative instead of the absolute slant TEC from the occultation antenna is used. Here absolute TEC means the leveled phase TEC to the pseudo range TEC, while relative TEC means the time difference of the phase TEC [Yue *et al.*, 2011b]. Figure 1 shows the year coverage and orbit altitude variations of the RO missions as well as those of Jason-1 and OSTM/Jason-2. Note that although the GRACE and SAC-C satellites were launched in 2002 and 2000, respectively, their operational RO observations were not activated till 2006 as shown in Figure 1. Except for CHAMP, all of the missions are working successfully now. Also shown in Figure 1 is the number of the daily available ground-based GNSS stations from the Crustal Dynamics Data Information System (CDDIS) international GNSS service (IGS) archive center [Noll, 2010]. Many more ground-based GNSS observations can be obtained from other IGS data centers. In this work we use only CDDIS IGS data since it is sufficient for the spatial resolution of the current study. We also plot the corresponding solar flux (F10.7) and geomagnetic activity (AP) indices in Figure 1 as a reference. Electron density profiles at noon and midnight over the equator obtained from the IRI-2007 model for a typical moderate solar activity condition are also shown in Figure 1. It is evident that the combined data sets from these satellites have a good coverage in the ionosphere *F* region [Bilitza, 2001]. In Figure 1 (bottom), we plot the number of daily occultation events accumulated at the UCAR/CDAAC. We can see that the total number of occultation events increases significantly after the COSMIC was launched.

[13] Each COSMIC satellite also has a tiny ionospheric photometer (TIP) payload, which can measure the OI 135.6 nm emission produced by ionospheric $O^+ + e$ recombination. This OI emission is nonlinearly related to the nadir-integrated electron density on the night side under some assumptions. We are not planning to use this data set in the current study because it has a relatively large observational uncertainty. Other ground-based observations, such as ionosonde and ISRs, are not used either, since ground-based GNSS observations already have a good coverage over land. These observations, however, will be used to validate the reanalysis outputs. A straight-line propagation assumption is used in all data processing, which makes the observation operator determination much more computationally efficient. In addition, it is not necessary to use the ray tracing here because the effects of the GNSS ray bending and separation are negligible given the coarse grid that is used and quiet situations are processed in the current study. We describe data

processing and quality control according to different categories in the following section.

2.1. Ground-Based GNSS Slant TEC

[14] The ground-based slant TEC calculation is relatively mature. Some institutions (e.g., JPL, MIT) automatically process global GNSS observations and release the results to the public [Komjathy *et al.*, 2005; Rideout and Coster, 2006]. However, most data centers only provide the gridded vertical TEC, which is less useful and less accurate than the original slant TEC for data assimilation purposes. In addition, it is not convenient to download these data for operational purposes. Thus we recently set up a ground-based slant TEC processing system at the UCAR/CDAAC. Essentially, our data processing follows the same procedures as other groups. GNSS observations obtained below 10° elevation angle are discarded to avoid multipath signals reflected from the ground. When calculating the phase TEC, we discard the GNSS arcs with TEC gradients larger than a certain value to avoid the effects of cycle slips. Since the pseudo range TEC noise decreases with the increase of the elevation angle, as shown by Mannucci *et al.* [1998], the pseudo range TEC is weighted by the corresponding elevation angle in the leveling. Figure 2 gives a comparison between the pseudo range TEC and the leveled TEC during 9/23/2009 from one IGS station processed at CDAAC, demonstrating that our leveling algorithm can give a reasonable leveled slant TEC.

[15] The GNSS satellite (GPS and GLONASS) DCBs are provided by the Center for Orbit Determination in Europe (CODE), which are obtained by a least squares fitting method based on the global ground-based GNSS observations [Schaer, 1999]. The GNSS satellites DCB are first calibrated by CODE results. The GNSS receiver DCBs are estimated by ourselves using the method proposed by Komjathy *et al.* [2005]. Specifically, it uses the GIM to estimate the DCBs. The ensemble average of four independent IGS centers' GIM (JPL, UPC, CODE, and ESA) is used in this study [Hernández-Pajares *et al.*, 2009]. For every GNSS slant TEC of one receiver, we assume that its vertical TEC at the pierce point is equal to the corresponding vertical TEC from the GIM and then treat the difference between two vertical TEC values as the DCB. So we can get one DCB for each slant TEC. The DCB of one receiver is assumed to be constant during 1 day. We can get lots of DCB for each receiver during 1 day. Then a daily average DCB is obtained for the specific receiver. Note that the DCB of GPS and GLONASS signals are solved separately for the GPS+Glonass receivers and can be quite different. The pierce point height is flexible and chosen to be 450 km in this study, which is the same as that of GIM construction. This method should give an accurate DCB estimation as long as the mixed GIM has no systematic bias. Validation shows that the GIM has a good quality at least over the land, where GNSS data are available [Hernández-Pajares *et al.*, 2009; Mannucci *et al.*, 1998]. From our test, this method can obtain reasonable DCB values. As an example, we compare the DCB provided by mixed GIM with that estimated by ourselves during 9/23/2009 for all the available IGS stations in Figure 3. Note that every center uses ~ 100 global GNSS stations to construct their respective GIM and some IGS stations are selected by more than one center. It is found that the GIM aided method can obtain very accurate DCBs and the root mean square error

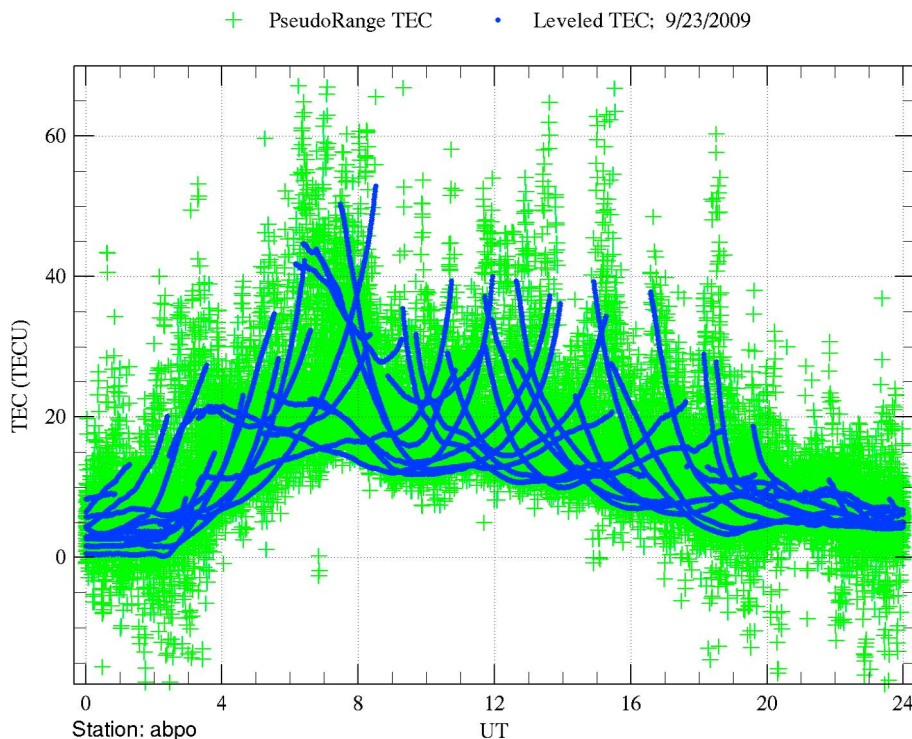


Figure 2. A comparison between the pseudo range TEC (green plus symbols) and the leveled TEC (blue solid circles) for the IGS station abpo during 23 September 2009. Note that both the GNSS satellites and the receiver DCB are already calibrated here.

(RMSE) between those obtained from the aforementioned four GIMs and our results is less than 3 TECU (1 TECU = 10^{16} electrons/m²). For ground-based receivers, the DCB usually has smooth variation with respect to time [Schaer, 1999]. However, the situation might be different for LEO receivers because of the movement of the LEO satellite as illustrated by Yue *et al.* [2011b]. Please note that all DCBs are calibrated before the data are assimilated into the model.

[16] Currently data from ~400 GNSS ground stations are available at the CDDIS IGS archive center. By adding data from other centers (e.g., GEONET, NOAA/CORS), the total number of stations could be increased to more than 2000 globally. Some of the stations can observe both GPS and GLONASS signals. In the current study, only GNSS observations from the CDDIS archive center are used. As shown in Figure 4d, the global GNSS stations give a good coverage over the land area with the exception of data gaps in the middle of Africa and in east Siberia.

2.2. Nadir Vertical TEC From Jason-1 and OSTM/Jason-2 Satellites

[17] Both the Jason-1 and OSTM/Jason-2 satellites are oceanography missions operated jointly by the National Aeronautics and Space Administration (NASA) of the United States and the Centre National d'Études Spatiales (CNES) (English: National Center for Space Studies) designed to monitor the sea surface topography. Both satellites orbits are almost circular at ~1336 km altitude and 66° inclination [Dumont *et al.*, 2009]. The dual-frequency Poseidon altimeters on board these satellites can be used to obtain the nadir

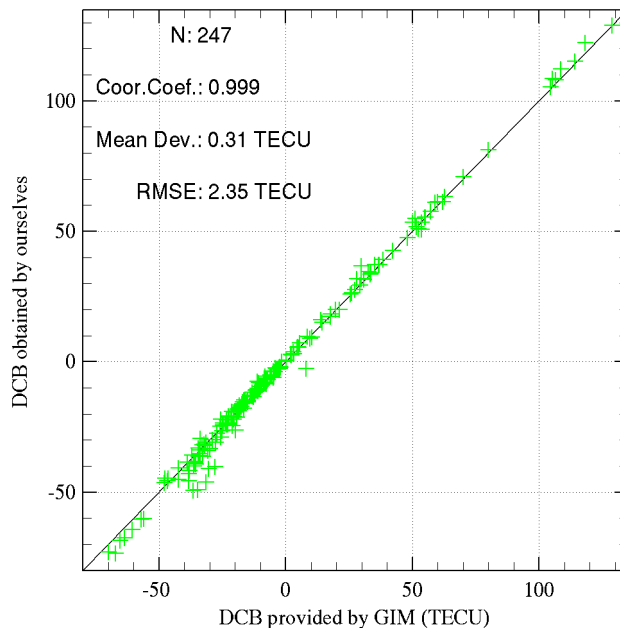


Figure 3. Comparison between the DCB provided by multi-GIMs (JPL, CODE, ESOC, and UPC) and the DCB estimated aided by ourselves during 23 September 2009 for IGS stations. The corresponding correlation coefficient, average deviation, and root mean square error are also given.

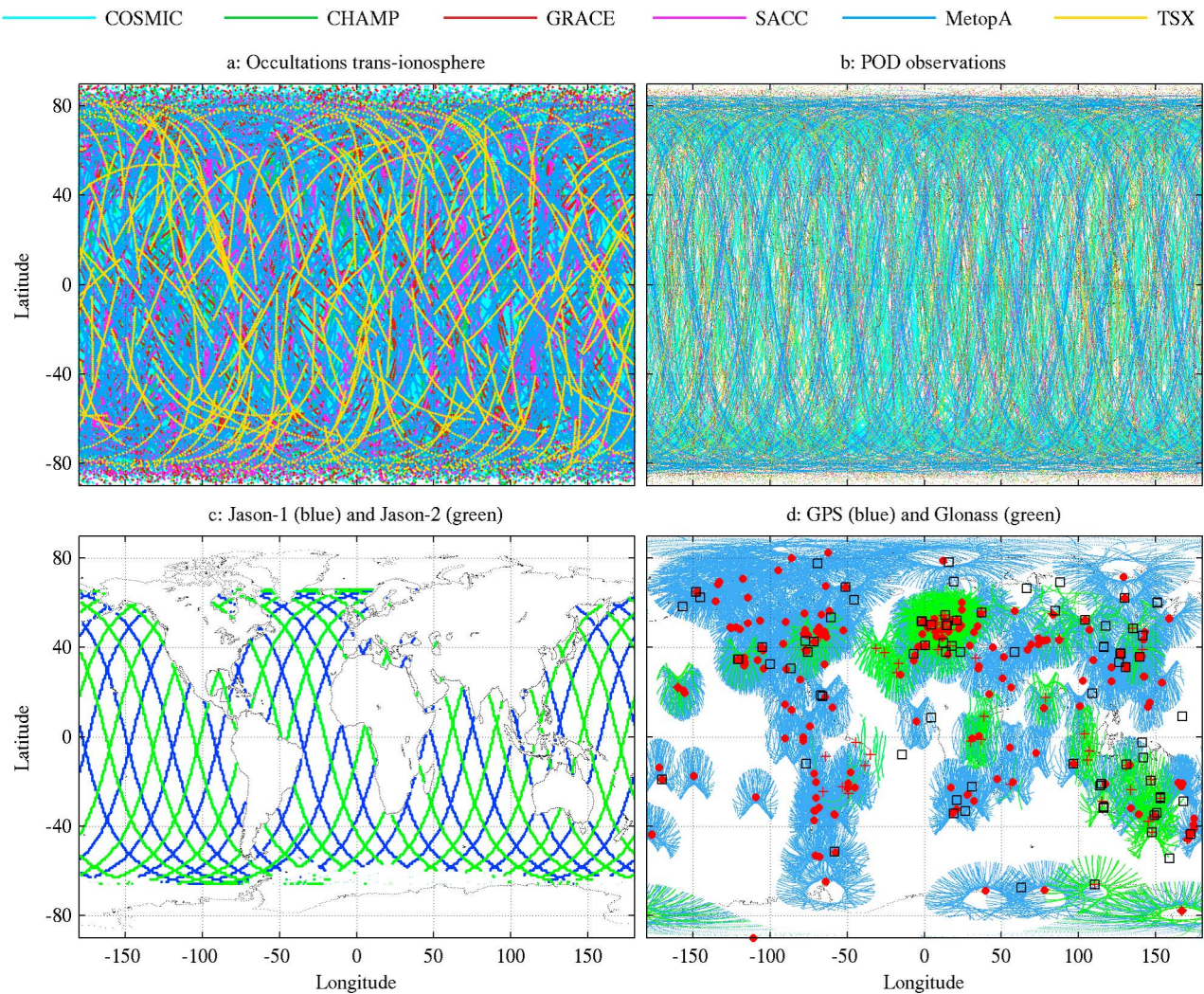


Figure 4. Daily coverage of (a) the transionospheric occultation GNSS rays and (b) POD antenna overhead observations (pierce point, altitude = 1000 km) from multiple radio occultation missions selected in this study. (c) Typical daily coverage of Jason-1 (blue) and Jason-2 (green). (d) Typical daily pierce points (450 km) coverage of ground-based GPS (blue) and Glonass (green) observations. The GPS stations (red open circles), GPS+GLONASS stations (red plus symbols), and the ionosonde stations (black square) used to do the evaluation are also shown.

vertical TEC between the sea surface and the satellite orbit altitude. In this work, the derived vertical TEC is smoothed with a 30 s window to reduce the observational uncertainty without sacrificing its accuracy according to *Imel* [1994]. The smoothed TEC is then assimilated into the model with a down-sampling rate of 15 s to avoid duplicate observations given the coarse grid in the study. As indicated by *Imel* [1994], the Jason vertical TEC might have a $\sim 2\text{--}3$ TECU hardware bias. Its effect can be ignored in this large-scale reanalysis study since its amplitude is within the uncertainty of most processed TEC [Yue *et al.*, 2011b]. Typical daily coverage of Jason-1 and 2 orbits are shown in Figure 4c. The altimeters provide high-resolution vertically averaged horizontal gradients of TEC along their tracks over the ocean regions during a monthly reanalysis given its 10 days repeat

period and complementary orbits of both Jason satellites [Dumont *et al.*, 2009].

2.3. Slant TEC From RO Satellites

[18] Absolute slant TEC used in the reanalysis includes data from the POD antennas of all the RO missions that are available at the UCAR/CDAAC (CHAMP, GRACE, SAC-C, COSMIC, TerraSAR-X, and Metop-A) and data from the occultation antenna of CHAMP [Jakowski *et al.*, 2002; Yue *et al.*, 2011b]. CHAMP, GRACE, and COSMIC have both overhead and occultation slant TECs, while SAC-C, TerraSAR-X, and Metop-A provide mainly the overhead slant TEC. LEO-based slant TEC processing at the CDAAC includes the cycle slip detection, multipath calibration, leveling of phase TEC to the pseudo range TEC by adding a constant value to the phase TEC, and DCB calibration. A detailed

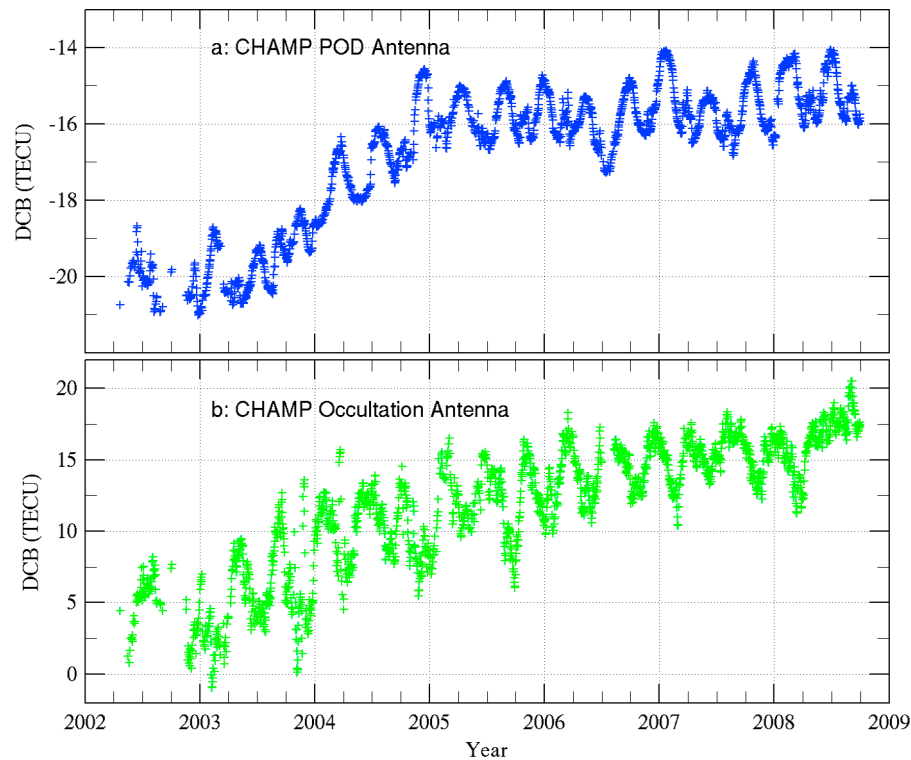


Figure 5. Daily DCB of (a) CHAMP POD and (b) occultation antennas from 2002 to 2009 estimated at the UCAR/CDAAC.

description about the CDAAC LEO slant TEC calculation can be found in *Yue et al.* [2011b]. In brief, the cycle slip is detected by the method suggested by *Blewitt* [1990]. The multipath of P1, C1, and P2 is obtained and calibrated based on a statistical analysis on a large number of the corresponding original observations. LEO TEC leveling is weighted by the corresponding signal-to-noise ratio (SNR), which is different from that of the ground-based GNSS processing. LEO receiver daily DCB is estimated by a least squares fitting solution of multiple simultaneous observation pairs under the assumption of spherical symmetry of the overhead ionosphere and a constant DCB during 1 day. As an example, Figure 5 shows the daily DCB of CHAMP POD and occultation antennas during 2002–2009 estimated at the UCAR/CDAAC. Both DCBs show a smooth day-to-day variability. The periodic variations and long-term drifts of both DCB values are resulted from the environment temperature variations caused by changes in satellite orbit cycles and solar flux [*Yue et al.*, 2011b]. A quantitative evaluation of the absolute slant TEC calculation is given in *Yue et al.* [2011b]. The accuracy of LEO slant TEC is $\sim 1\text{--}3$ TECU, depending on the satellites design [*Yue et al.*, 2011b].

[19] The phase TECs from the occultation antennas of GRACE, SAC-C, TerraSAR-X, and Metop-A are also used in the reanalysis. The DCB of the CHAMP occultation antenna can be calibrated well based on the spherical symmetry assumption since the CHAMP occultation antenna can track GPS signals up to the elevation angle of $\sim 5^\circ$ [*Yue et al.*, 2011b]. The COSMIC POD antenna already gives occultation TEC down to the Earth surface. So it is not necessary to use the relative TEC from these two missions. The phase TEC

has an accuracy of ~ 0.01 TECU [*Schaer*, 1999]. Table 1 summarizes the data types used in the reanalysis for each instrument.

3. Global Ionospheric Data Assimilation Model Description

[20] This global ionospheric data assimilation model has been developed based on some of our previous studies [*Yue et al.*, 2007a, 2007b, 2011a]. The key parameters of the model, including spatial and temporal resolutions, background and observation covariances, and background models, can be customized by the user. Different from that of atmospheric

Table 1. Summary of the TEC Types (Absolute or Relative) of Each Instrument Used in the Reanalysis

		Absolute TEC	Relative TEC
Ground GNSS		✓	
Jason-1/2		✓	
CHAMP	POD	✓	
	OCC.	✓	
GRACE	POD	✓	
	OCC.		✓
SAC-C	POD	✓	
	OCC.		✓
COSMIC	POD	✓	
	OCC.		
TerraSAR-X	POD	✓	
	OCC.		✓
Metop-A	POD	✓	
	OCC.		✓

reanalysis, which usually use theoretical model as background, we will use an empirical model as background here. In this study, the selected background model is the IRI2007 model with the International Union of Radio Science (URSI) N_mF_2 and the International Radio Consultative Committee (CCIR) h_mF_2 maps and the NeQuick topside option [Bilitza, 2001; Bilitza and Reimisch, 2008]. The model grid spatial resolution is 5° in latitude, 10° in longitude, and 30 km in altitude from 70 to 1000 km and 100 km from 1000 to 2000 km. The plasmasphere above 2000 km is provided by the Gallagher H^+ model [Gallagher *et al.*, 1988]. The background model error is assumed to be the square of the background and the error is spatially Gaussian correlated [Yue *et al.*, 2007a, 2007b]. Specifically, the correlation distance is 2 times larger in the daytime (12:00) than at night (00:00). The meridional correlation is larger in the middle latitude than both high and low latitudes, with typical value of 14° in 45° latitude and 8° in 0° and 85° latitudes. The zonal correlation distance linearly increases from 10° in the equatorial area to 40° in the polar region. The vertical correlation exponentially increases from ~ 50 km in 100 km altitude to ~ 600 km in 2000 km altitude [Yue *et al.*, 2011a]. The background covariance is set to be 0 when the distance between two grid points is longer than 1000 km. The observation error is assumed to be uncorrelated and its amplitude is far less than that of the background since we trust the observations more than the model. The assimilation is performed using a Kalman filter method [Yue *et al.*, 2011a]. It is the standard Kalman filter except not considering the time forward of the covariance in the Kalman filter, which means that previous observations will have no effect on the current assimilation estimation. So the assimilation will obtain a global optimization by minimizing the difference between the model and the various observations. We carried out a series of simulation studies recently based on this model [Yue *et al.*, 2012b]. It is found that the global data assimilation can improve the Abel inversion and offers an optimal RO electron density profile retrieval if sufficient ROs are available simultaneously [Yue *et al.*, 2012b].

[21] The observation operator is the integration along the GNSS raypath when the absolute slant TEC is assimilated. For the phase TEC, its time difference is assimilated. The corresponding observation operator is the difference of the integration along two adjacent GNSS rays. By assimilating the time difference of the phase TEC we actually assume that the background model is unbiased. We prefer to assimilate the absolute slant TEC if it is available. All the assimilated TEC values are first quality controlled by identifying outliers, by detecting cycle slips, by value range restriction, and by removing bad GNSS arcs. Duplicate GNSS rays, which pass through exactly the same grid points, are also removed.

4. Preliminary Reanalysis Results

[22] The time resolution of the reanalysis is flexible. Since satellite-based observations are not sufficient for a daily reanalysis, especially before the COSMIC data were available, we carry out a monthly reanalysis with 1 h time resolution from 2002 to 2011 in this preliminary study. For a given month, only data from days with a daily AP index less than 15 are combined and we do the global 3-D reanalysis for each UT hour separately. So the reanalysis output is 24 3-D

(spatial resolutions of 5° in latitude, 10° in longitude, and ~ 30 km in altitude) electron densities for each month and for each hour in the “average” day. All satellite observations shown in Figure 1 (only quiet days are used) are assimilated simultaneously for the given month and UT. For a ground-based GNSS station, only the quietest day of the month is selected because its observation configuration does not change too much during 1 month. We, in fact, ignore the ionospheric day-to-day variability during the month here. This will not affect our climatological results, such as seasonal and solar cycle variations.

[23] As an example, we show a typical daily coverage by occultation transionospheric rays (Figure 4a) and overhead POD observations (Figure 4b) from multisatellite missions in Figure 4. There is a very good global coverage of the ionosphere by combining all these RO data together. Also shown in Figure 4 is the typical daily coverage by Jason-1/2 satellites and by the ground-based GNSS observations, which provide ionospheric horizontal information over the ocean and land area, respectively.

[24] As a first step to evaluate the effectiveness of our assimilation scheme, we compare the observed slant TEC, which is assimilated into the model, with the corresponding a priori (before assimilation) and a posteriori (after assimilation) results. Figure 6 shows two such comparisons for high and low solar activity conditions, respectively. From both the scattered plots (Figure 6, left) and the statistics of the differences (Figure 6, right), we can see that the a posteriori TEC is closer to the observed TEC than the a priori TEC is. The difference for the a posteriori TEC also has a narrower Gaussian distribution. The correlation coefficient and RMSE is 0.9 and ~ 20 TECU between the a priori TEC and the observed TEC for the 2002 case and 0.93 and ~ 22 TECU for the 2008 case. The corresponding value is 0.99 and ~ 5 TECU for 2002 and 0.99 and 5.5 TECU for 2008 between the a posteriori TEC and the observed TEC. For the low solar activity case of November 2008, although the background model on average overestimates the TEC by ~ 5.7 TECU, the assimilation still can give an unbiased a posteriori result with an average deviation less than 0.1 TECU (average difference between a posteriori and observed TEC).

[25] Figure 7 gives an example of the reanalyzed global 3-D electron density as well as N_mF_2 and the vertical TEC map at 1900 UT in September 2006. The reanalyzed results show reasonable large-scale ionospheric features, such as the spatial and temporal evolution of the equatorial ionization anomaly (EIA), the nighttime middle latitude electron density trough, and the hemispheric asymmetry. Specific validation results will be given in the following section.

5. Validation Results

5.1. Comparing the Reanalyzed N_mF_2 With RO Retrieved Results

[26] As pointed out by Liu *et al.* [2010] and Yue *et al.* [2010], the Abel retrieval can give a very accurate ionospheric peak height (h_mF_2) and peak density (N_mF_2) from the RO measurements. But it tends to smooth out the EIA structure because of the spherical symmetry assumption. This results in an underestimation of the EIA peak and an overestimation of the EIA trough and therefore a less evident

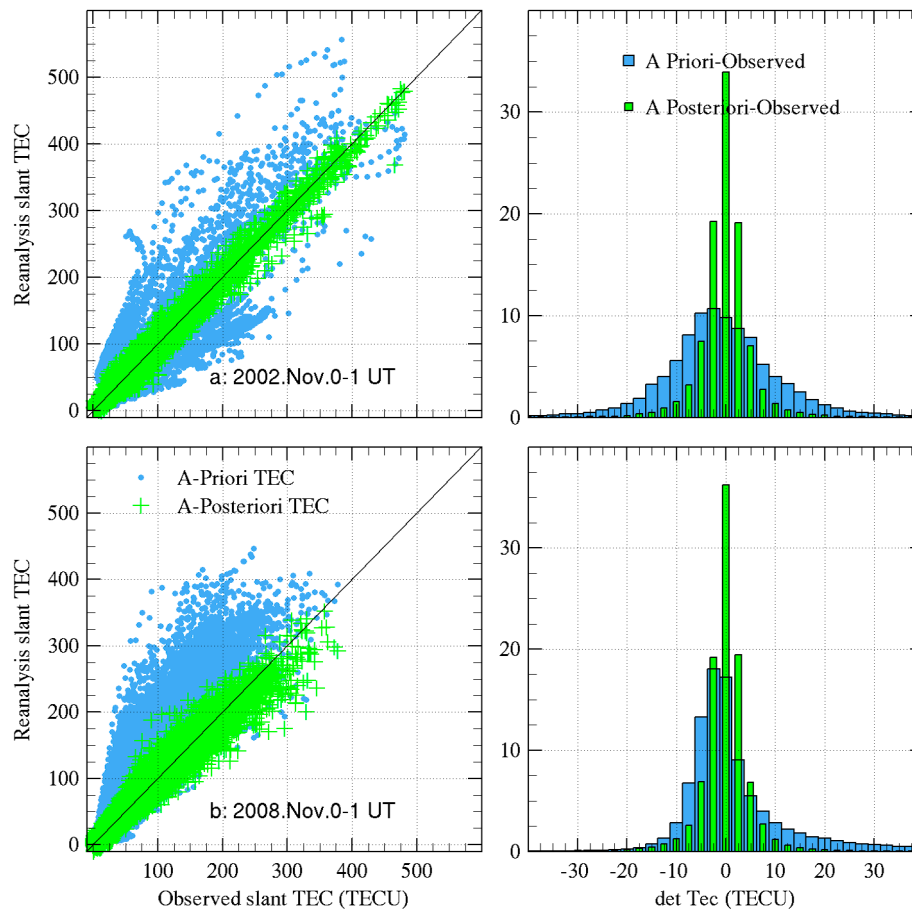


Figure 6. Comparison of the observed slant TEC with the a priori and a posteriori TEC of the reanalysis at UT = 0–1 for (a) November 2002 and (b) November 2008, respectively. On the right are the corresponding statistical results of the left.

EIA. Figure 8 shows the local time and magnetic latitude variation of global $N_m F_2$ in February 2009 from COSMIC RO Abel retrieved electron density profiles, the reanalysis results, and the IRI model, respectively. As can be seen, RO retrievals, reanalysis, and the IRI model have similar local time and latitude patterns. In comparison with RO retrievals, the reanalysis results have better defined and more evident EIA, as discussed above. On the other hand, the IRI model significantly overestimates $N_m F_2$ in comparison with either the RO retrievals or the reanalysis. The overestimation of ionospheric electron densities by the IRI during the 23/24 solar minimum has been reported in a few recent studies [e.g., Lühr and Xiong, 2010; Yue et al., 2012a]. Our reanalysis results are consistent with those studies.

5.2. Validation Using the IGS GIM Global Electron Content

[27] *Afraimovich et al.* [2006] proposed a global electron content (GEC) index to represent the global ionosphere condition. To validate our reanalysis results, we calculated the monthly average GEC indices from the reanalysis, the IRI model, and the IGS mixed GIM, following the same method as that of *Afraimovich et al.* [2006]. The same quiet days that are used by the reanalysis are employed in calculating the monthly GEC index of the IGS mixed GIM. Each

IGS GIM is created from the ground-based GNSS observations under a thin layer assumption [*Mannucci et al.*, 1998]. It might have a degraded performance over the ocean region because of the limited data coverage. But it at least can represent the large-scale ionosphere morphology statistically and can be used to evaluate the reanalysis results. The corresponding comparison and statistical results are given in Figure 9.

[28] Generally, the three GEC indices show similar solar activity and seasonal variations. Compared with the IGS GIM GEC, the reanalysis GEC has a better performance than the IRI-modeled GEC in terms of both the temporal variation of the deviations and the statistical results of the deviations. The correlation coefficient, average deviation, and RMSE between the reanalysis GEC and the IGS GIM GEC are 0.97, 0.88 GECU (1 GECU = 5.77×10^{30} electrons), and 1.8 GECU, respectively, whereas the corresponding values between the IRI model and the IGS GEC are 0.95, 2.55 GECU, and 2.2 GECU, respectively. During the solar minimum of 2007–2009 the IRI model overestimates the GEC by up to 20–30%. On the other hand, this overestimation can be well corrected by assimilating multiple sources observations, as indicated by the small differences between the green and blue lines in Figure 9. After April 2006, when the COSMIC satellites were launched, the reanalysis has a much better agreement with the

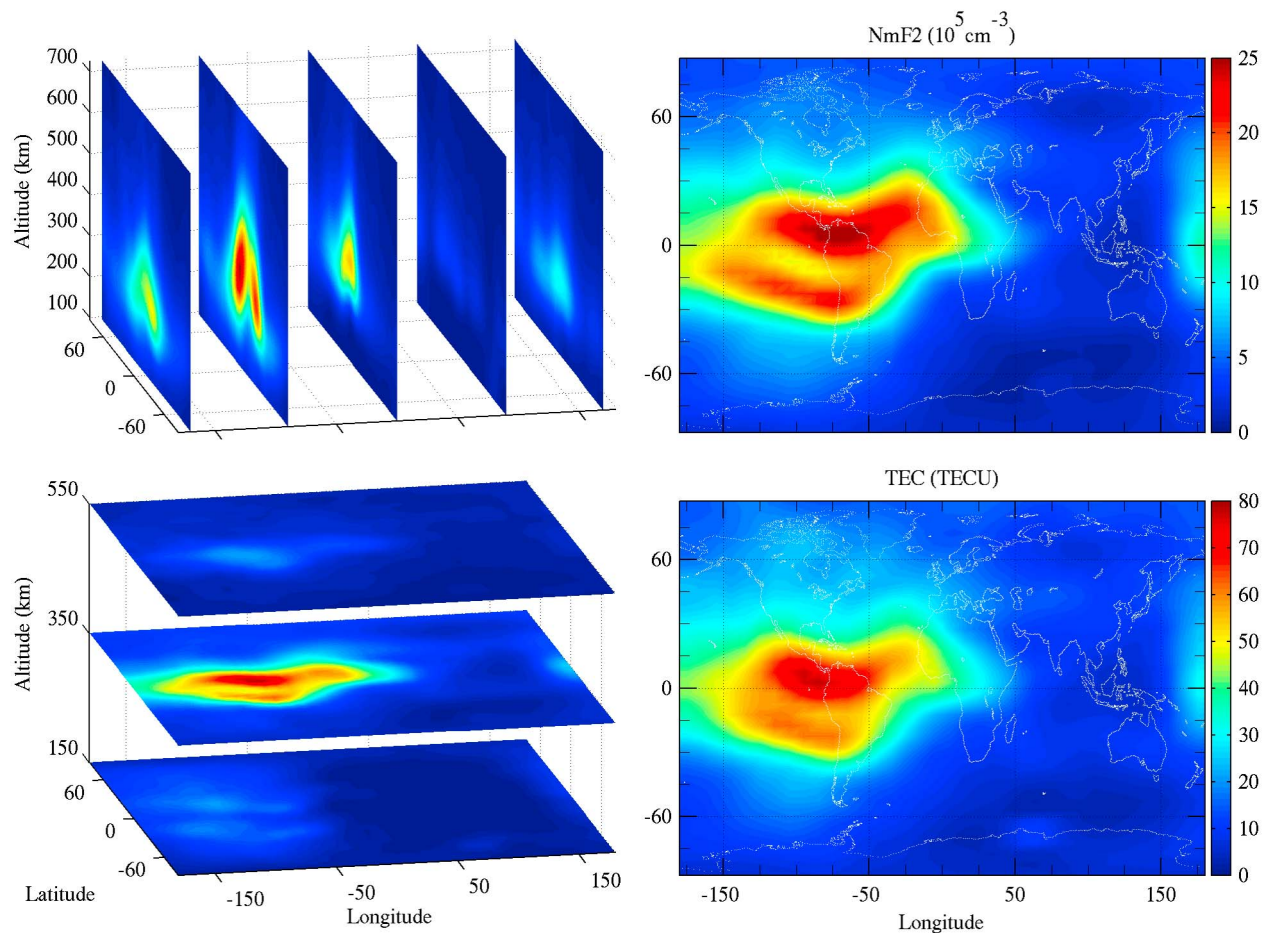


Figure 7. Example of the reanalyzed global 3-D electron density and the corresponding peak density (N_mF_2) and vertical TEC map at 1900 UT in September 2006.

IGS GIM results than before the COSMIC launch, as more RO data evidently improve the reanalysis results.

5.3. Validation by the Poker Flat ISR Electron Density Profiles

[29] The ISR provides the most accurate measurements of the whole ionospheric electron density profile from the ground. However, most ISRs operate infrequently because of relatively high operational costs. Fortunately, the newly built Poker Flat ISR (PFISR) (65.07°N , 147.28°W) operated almost continuously during this solar minimum (2007–2010) for the international polar year (IPY) campaign [Sojka *et al.*, 2009]. This offers a unique opportunity to validate the reanalysis results using an independent data source, albeit at only one location at high latitudes. We select only quiet day ($AP < 15$) observations and calculate the monthly median electron density profiles for every hour. The reanalysis results are then interpolated to the Poker Flat location to make comparisons.

[30] Figure 10 compares the PFISR observed monthly median electron density profiles with those interpolated from the reanalysis results during 2007–2010. Generally, the reanalysis results follow the same altitude, local time, and seasonal variations as the PFISR electron density profiles. In

particular, the reanalysis can reproduce well the electron density profiles below the F_2 peak. Both PFISR and reanalysis show high electron densities from 100 km to about the F_2 peak (~ 250 km) in summer. This is a significant improvement over the Abel retrieved RO electron density profiles which tend to have large errors and sometimes totally erroneous results below the F_2 peak [Yue *et al.*, 2010]. The obvious large enhancement in PFISR electron densities during July and August in 2010 might be related to ISR data quality or to contamination by auroral precipitation.

[31] Figure 11 gives the local time and altitude variations of the average deviations (2007–2010) of the reanalysis (Figure 11a) and the IRI model (Figure 11b) from the PFISR observations. The IRI model overestimates the electron densities during daytime in the F_2 peak region and underestimates them at the nighttime in the lower ionosphere. On the other hand, the overall amplitude of the deviations between the reanalysis results and the PFISR observations is much smaller. The maximum amplitudes of the average overestimation (underestimation) is $0.55 \times 10^5 \text{ cm}^{-3}$ ($0.61 \times 10^5 \text{ cm}^{-3}$) for the IRI model and $0.15 \times 10^5 \text{ cm}^{-3}$ ($0.25 \times 10^5 \text{ cm}^{-3}$) for the reanalysis results, respectively. During most of the times and over almost all altitudes, the

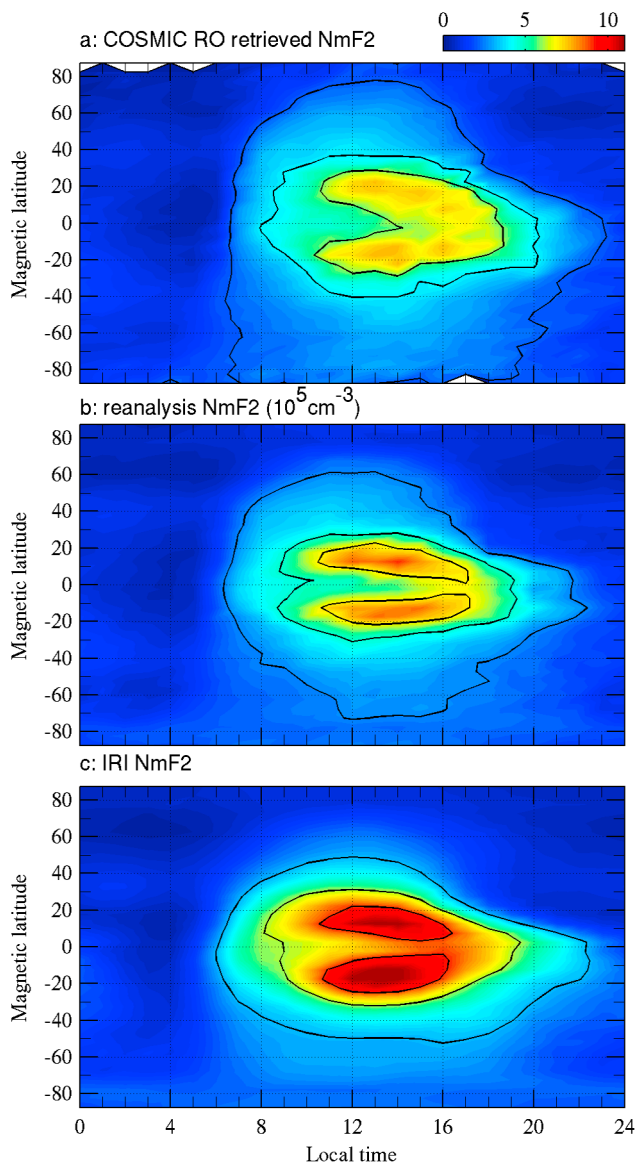


Figure 8. Local time and magnetic latitude variation of global $N_m F_2$ from (a) COSMIC radio occultation retrievals, (b) reanalysis results, and (c) the IRI model during February 2009.

deviations of the reanalysis are around 0, except around noon in the lower ionosphere. This is probably due to some small-scale structures in the high-latitude region.

5.4. Validation by Global Ionosonde Observations

[32] Ionosondes can continuously measure the ionospheric electron density, especially the ionospheric critical frequency ($f_o F_2$) with very high accuracy. In this study, global ionosonde-observed $f_o F_2$ values from the National Oceanic and Atmospheric Administration's (NOAA) National Geophysics Data Center (NGDC) from 2002 to 2011 are used to evaluate the reanalysis results. The number of the available global ionosonde stations with data at NOAA/NGDC increased from ~ 20 in 2002 to ~ 60 in 2011. Some stations did not operate continuously. Thus the number of the

available stations actually changes from month to month. In Figure 4d we use black squares to represent all the available ionosonde stations from 2007 to 2011 (~ 70 in total). Please note that modern ionosondes scale $f_o F_2$ automatically while older ionosonde scaling was done manually. This does not influence the data quality when calculating monthly median by using only quiet days' data. For each month at each station, the same quiet days as selected in the reanalysis are used to calculate the monthly median $f_o F_2$. The reanalysis results are then interpolated to the corresponding stations to make comparisons.

[33] Figure 12 shows a comparison of the ionosonde $f_o F_2$, the IRI $f_o F_2$, the reanalysis $f_o F_2$, as well as the deviations of the IRI and reanalysis $f_o F_2$ from that of the ionosonde at Townsville (19.63°S , 146.85°E). Generally, the three $f_o F_2$ show similar solar activity, seasonal, and local time variations. The reanalysis $f_o F_2$ has smaller deviations than the IRI model $f_o F_2$, especially after the COSMIC satellites were launched in April 2006, and therefore more RO data were available. Specifically, the overestimation of $f_o F_2$ by the IRI model during the daytime and at sunset after April 2006 is not seen in the reanalysis. We made this comparison station by station. Generally, the conclusion is similar to the example shown in Figure 12.

[34] Figure 13 gives the statistical results of the deviations of the IRI model and reanalysis $f_o F_2$ from all available ionosonde $f_o F_2$. Since the improvement by the reanalysis is not significant before the availability of the COSMIC data, only the results from 2007 to 2011 are used here. Obvious improvement by the reanalysis can be seen in comparison with the IRI model results. The overall average deviation, correlation coefficient, and RMSE are (0.11 MHz, 0.94, 0.69 MHz) for the IRI model and (-0.006 MHz, 0.96, 0.51 MHz) for the reanalysis, respectively. Specific local time and magnetic latitude variations of the corresponding mean deviation, RMSE of the deviations, mean relative deviation, and RMSE of the relative deviations are given in Figure 14. Indicated from either the mean deviation or the RMSE of the deviations in terms of either absolute or relative deviation, the reanalysis results improved the IRI model predictions. In terms of mean relative deviation, although the IRI model already has a good prediction performance with the error in $\pm 25\%$ level, the reanalysis results reduce the error to be in $\pm 10\%$. During nighttime, the IRI model has larger RMSE than that of the reanalysis.

6. Discussion

[35] In this study, multisource, quiet-day, slant TECs are assimilated into the background IRI-2007 model to obtain a monthly mean reanalysis of the ionosphere from 2002 to 2011. The reanalysis results are given in three dimensions and cover all local times. We validate the reanalysis with COSMIC RO retrievals, IGS GIM, and several independent observations that included the PFISR observed electron density profiles and the global ionosonde observed $f_o F_2$. All the comparisons show that the reanalyzed electron density is closer to the observations than the IRI model predictions. This is especially true after April 2006, when RO data are available from the COSMIC mission. Our validation shows that the assimilation of RO data into the IRI model results in significantly improved agreement with independent data.

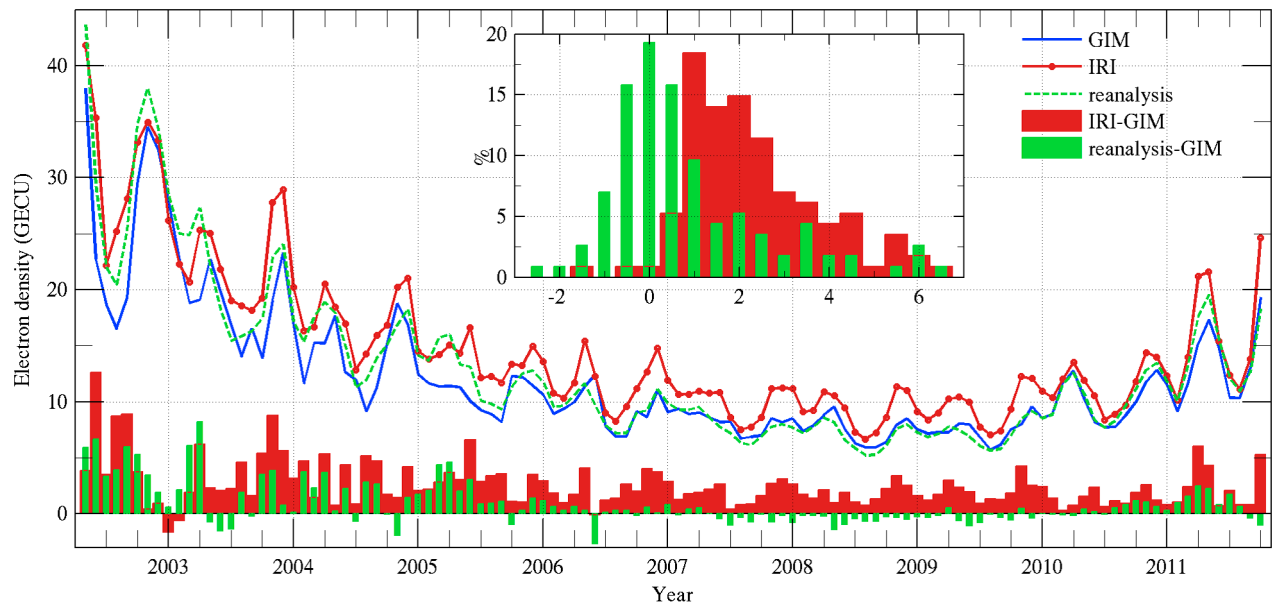


Figure 9. Comparison of global electron contents (GEC, $1 \text{ GECU} = 5.77 \cdot 10^{30}$ electron) between the IGS mixed GIM (blue line), the IRI model (red line with dot), and the reanalysis results (green dashed line) during 2002–2011. The difference between the IRI and the GIM (red bar) and between the reanalysis and the GIM (green bar) and their corresponding statistical results are also given (insert).

[36] During the 23/24 solar minimum (2007–2009), the IRI model tended to overestimate electron densities in the region just above the *F* peak [Lühr and Xiong, 2010; Yue et al., 2012a]. IRI is an empirical model and its accuracy for specific conditions therefore depends on the availability of

prior data for similar conditions. Because of the uniqueness of the recent solar minimum there are no prior data taken under similar conditions, and it is therefore not surprising that IRI overestimated the measurements [Bilitza and Reinisch, 2008; Solomon et al., 2010, 2011]. The reanalysis gives a

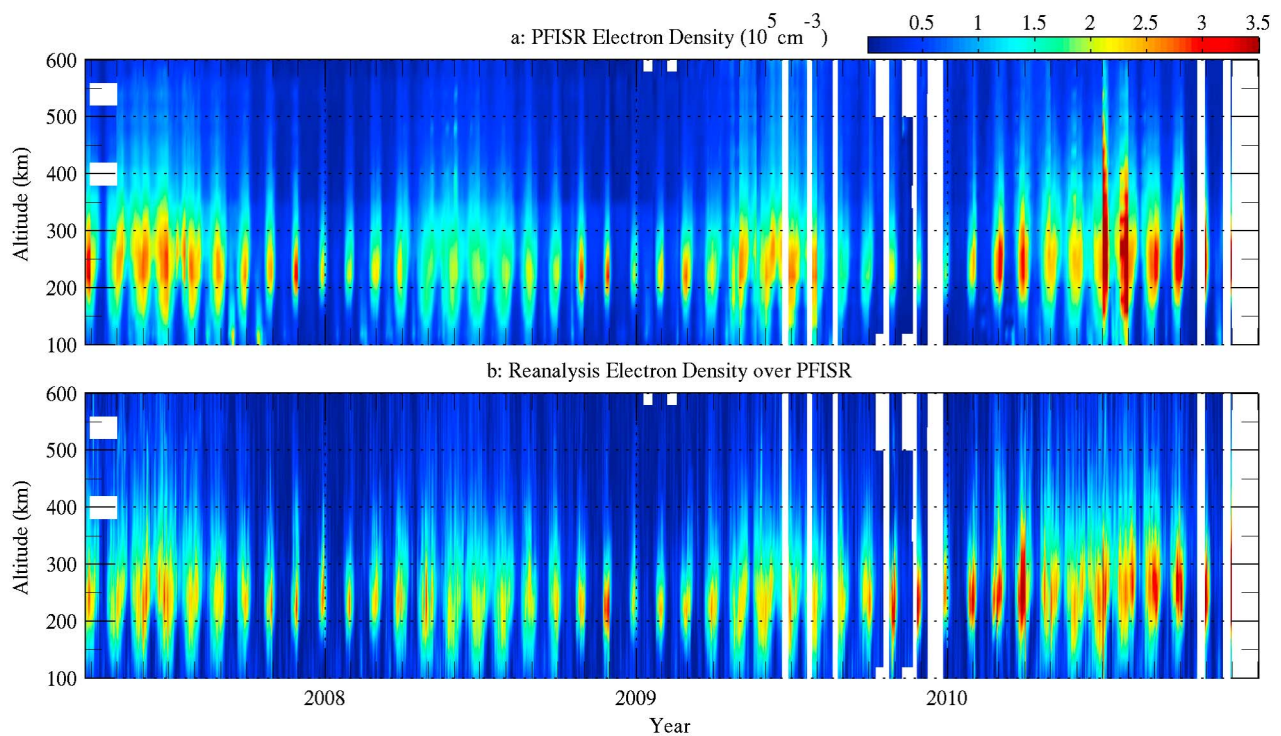


Figure 10. Comparison of (a) Poker Flat Incoherent Scatter Radar (PFISR) observed monthly electron densities with (b) the reanalysis results during 2007–2011.

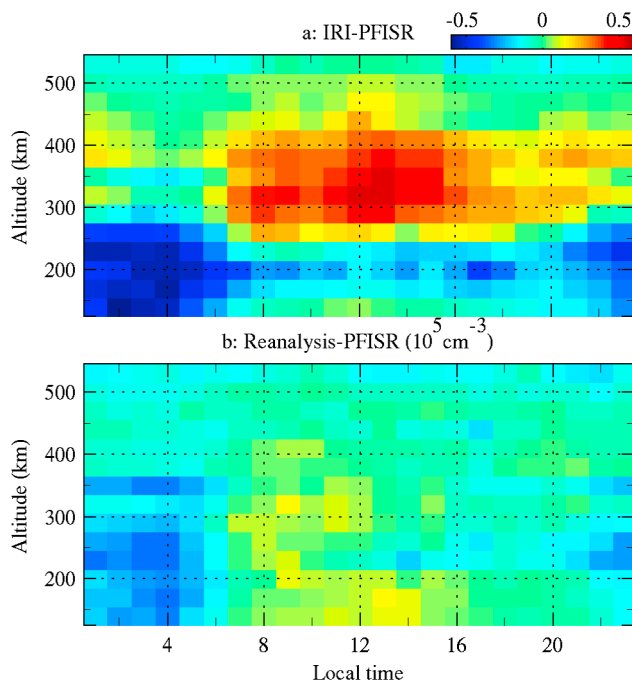


Figure 11. Statistical average deviations of (a) the IRI modeled and (b) the reanalysis monthly electron densities from those of PFISR observations.

better description of the global ionosphere electron density over the last solar minimum by constraining the background model (IRI) predictions with RO and TEC observations. The IRI model has different options for specifying the topside ionosphere. Our assimilation model is based on the standard IRI-2007 model which uses the NeQuick option for the topside [Bilitza and Reinisch, 2008]. Using a different topside option might lead to different results [Yue *et al.*, 2012a].

[37] In this study, we only do the reanalysis for the quiet ionosphere. The results can be mainly used to study the ionospheric climatology. Please note that the climatology in this reanalysis might be influenced given the day-to-day variation is ignored. In addition, those variations with period less than 1 month cannot be identified well. During disturbed conditions, the ionosphere can have significant and complicated disturbances with different spatial and temporal scales, which imply that higher model resolution in both space and time and more data are needed to get an accurate data assimilation estimation when disturbance are present. In addition, the background model whether empirical or physics-based will have degraded prediction ability during nonquiet situations.

[38] Figures 11, 12, and 14, however, do show that at certain local times and locations the reanalyzed electron density still deviates significantly from the independent observations. This is probably due to the following.

[39] 1. The first reason is the uncertainties of the independent observations. The IGS GIM, the ionosonde and ISR all have their own uncertainties in data retrievals.

[40] 2. The second reason is the procedure of interpolating the reanalysis data to the observation location and time. The current reanalysis has a relatively low spatial and temporal resolution (5° in latitude, 10° in longitude, 30 km in altitude,

and 1 h in time). When doing the interpolation, it may result in some uncertainties.

[41] 3. The third reason is uncertainties in the observations that are being assimilated into the background model and inconsistency among different observation types. Each observation type has its own data processing procedures and therefore unequal errors and bias. When all the data are assimilated simultaneously during a certain time period, the reanalysis result is actually a global optimization by minimizing the difference between the model and various observations. It might have some deviations when compared with other types of observations.

[42] 4. The fourth reason is insufficient and/or inhomogeneous coverage with the assimilative data. The error of the reanalysis is reduced significantly when more RO data are included after the COSMIC data are available. We expect that the reanalysis will give more accurate results in the near future when more ground-based and space-based TEC and RO data from missions such as COSMIC 2 will be available [Yue *et al.*, 2012b].

[43] In addition to including more data into the reanalysis, there are other areas that can improve the model.

[44] 1. In this study, we use a Gaussian correlation of the background and the correlation distance follows the statistical results of Yue *et al.* [2007b]. As indicated by Bust *et al.* [2004], more detailed research on the ionospheric spatial correlation is needed to better define the background covariance and the impact zone.

[45] 2. We used only slant TECs from the ground-based GNSS stations, POD and occultation antennas of RO missions, and Jason-1/2 altimeters in this reanalysis. Other type of data, including global ionosonde and ISRs observations, satellite in situ measurements, and airglow emission, should be incorporated in future studies. Furthermore, we consider only one ionospheric parameter, electron density, in this study. Other ionospheric parameters such as plasma temperature and drift can be reanalyzed as well. These parameters are critical for understanding the morphology as well as the variability of the ionosphere and thus are of great importance in both scientific research and application.

[46] 3. The uncertainties in either the model or the observations are represented in a very simple way in this study. To increase the accuracy of the reanalysis, both the model and the observation uncertainties should be handled in a more robust way. For the model, its uncertainties can be derived from statistical comparisons with highly accurate, real observations. For each type of data, their uncertainties can be obtained from data processing and validation [Yue *et al.*, 2011b].

[47] 4. In the current study, we did not propagate the error covariance forward in the Kalman filter because we do the monthly reanalysis and use an empirical model as background. It implies that the previous observations will have no effect on the current reanalysis. In the future, the covariance should be forwarded in time if the reanalysis are implemented continuously.

[48] 5. The current study is actually a demonstration study. When more data are available, the reanalysis can be implemented on a daily basis with much higher spatial and temporal resolution. Thus it can also perform nowcast of the ionospheric weather, not just the ionospheric climatology that is presented in this paper. In addition, first principles models of the coupled thermosphere ionosphere system, such as the

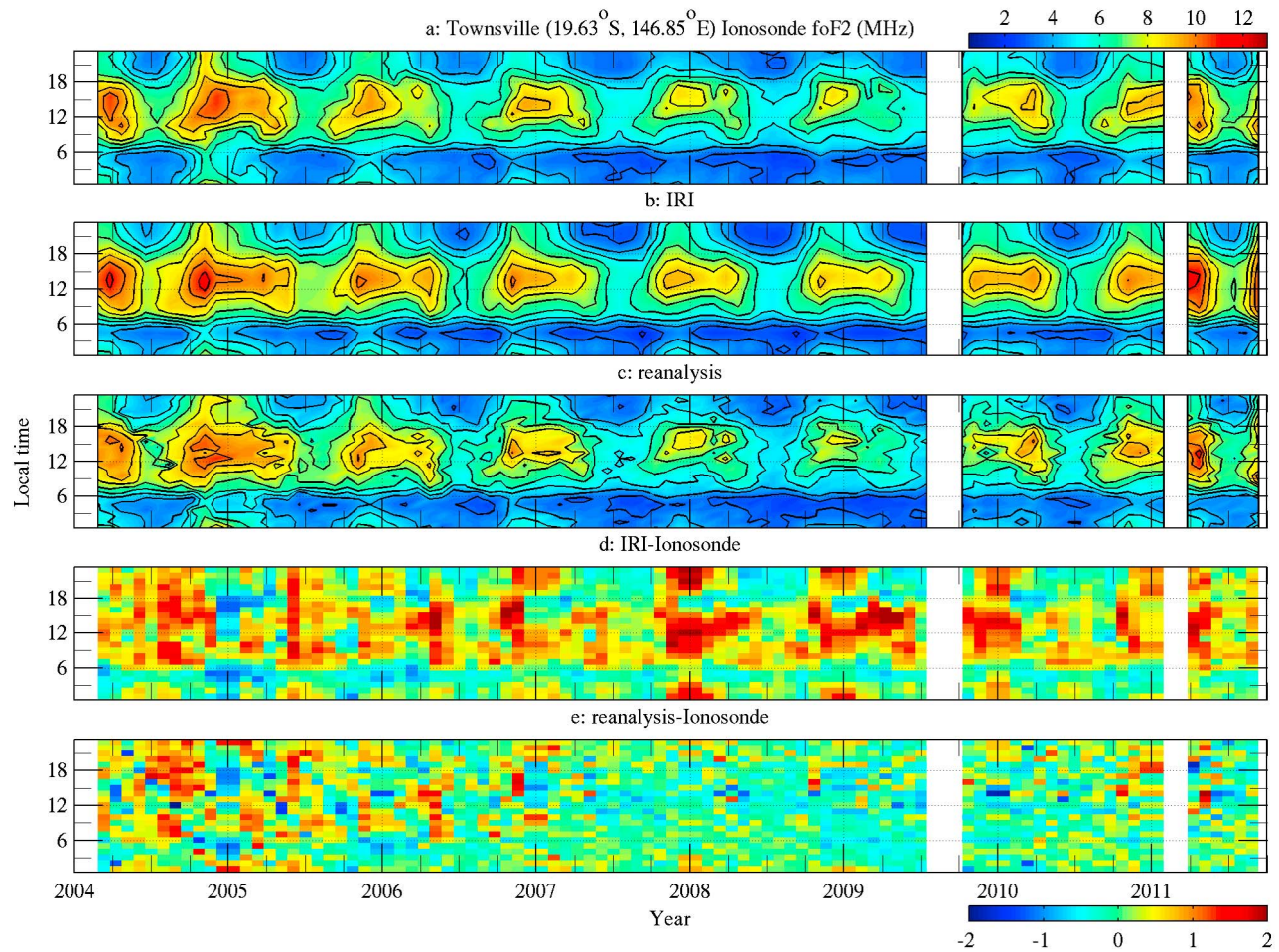


Figure 12. Comparison of monthly f_oF_2 (MHz) between (a) the ionosonde observations, (b) the IRI model, and (c) the reanalysis interpolated results over Townsville (19.63°S , 146.85°E) during 2004–2011. Also shown is the difference between (d) the IRI and ionosonde results and (e) the reanalysis and ionosonde results.

thermosphere ionosphere nested grid (TING) version of the NCAR-thermosphere ionosphere electrodynamics general circulation model (NCAR-TIEGCM), will also be employed as the background model to enhance the short-term forecast capability [Wang *et al.*, 1999].

[49] The ionospheric reanalysis using multisource data developed in this study can have significant impact on both space science research and application.

[50] 1. The reanalysis method can make full use of multisource ionospheric observations, especially those that are difficult to use directly in scientific research and the applications. The reanalysis outputs of the gridded ionospheric electron density can be used for ionospheric research as well as ionospheric weather monitoring [Burns *et al.*, 2008].

[51] 2. An accurate nowcast and forecast of the ionospheric electron density is always important for ionospheric applications. The ionospheric correction plays a crucial role in radar and satellite communications for better timing or positioning. Reanalysis is a viable approach to realize an accurate

nowcast of the ionosphere by assimilating all the available data in a systematic way. In addition, it extends the traditional 2-D ionospheric TEC map to a 3-D ionospheric electron density distribution and thus enables the studies of the global three-dimensional variability of the ionosphere to be made. In the near future, more ionospheric data, especially the RO data from space missions such as the COSMIC follow-up, will become available [Yue *et al.*, 2012b]. This offers us an unprecedented opportunity to make the near real-time, accurate 3-D ionosphere nowcast and forecast possible.

[52] 3. These electron density reanalysis can be used to calibrate the large-scale ionospheric residuals on the lower-atmosphere RO retrieval [Mannucci *et al.*, 2011]. This will also benefit lower-atmosphere climate studies.

7. Conclusion

[53] In this paper, a global ionospheric data assimilation model that uses a Kalman filter method and the IRI model have been described. A data processing function of both the

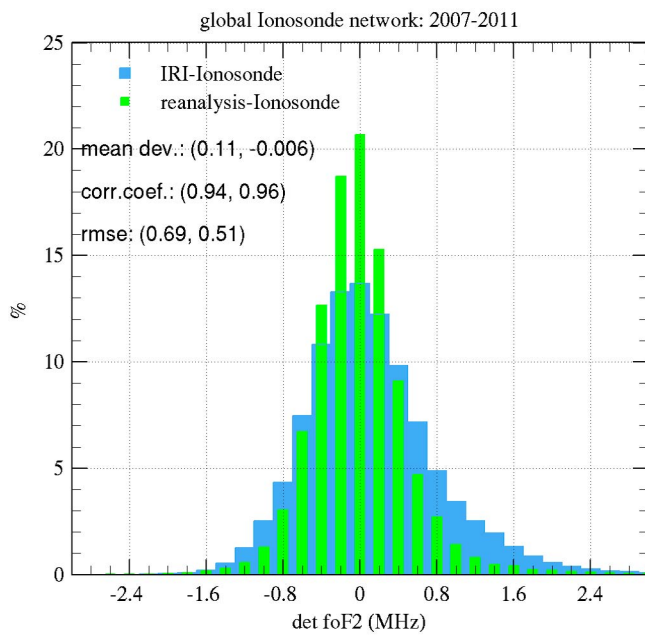


Figure 13. Statistical results on the deviations of the IRI modeled (blue bar) and the reanalysis interpolated monthly f_oF_2 (green bar) from that of global 70 ionosonde stations measurements during 2007–2011. The corresponding average deviation, correlation coefficients, and the root mean square error (RMSE) of the deviations are also displayed in the brackets (IRI, reanalysis).

ground-based and LEO satellite based GNSS observations is embedded in this assimilation model. We then used this model to reanalyze the monthly global 3-D ionospheric electron density from 2002 to 2011 by assimilating the quiet-day observations from ground-based GNSS stations, GPS observations from CHAMP, GRACE, COSMIC, SAC-C, Metop-A, and TerraSAR-X satellites, and nadir vertical TEC from Jason-1/2 altimeters. The reanalysis output consists of 3-D gridded electron densities with temporal and spatial resolutions of 1 h in universal time, 5° in latitude, 10° in longitude, and ~ 30 km in altitude. IGS GIM derived GEC, PFISR observed electron density profiles from 2007 to 2010, and global ionosonde network observed f_oF_2 from 2002 to 2011 are used as independent data to validate the reanalysis results. The climatological features of the reanalysis results, including solar activity and seasonal variations, and the global morphology of the ionosphere, agree well with empirical models and observations. All the comparisons show that the reanalysis results have smaller deviations from the observations than the background model. The accuracy of the reanalysis field significantly improves after April 2006, when the six COSMIC satellites were launched, and thus much more RO data became available. The obvious overestimation made by the IRI model during the 23/24 solar minimum is corrected well by the assimilation. The reanalysis model therefore is a good candidate for the efforts undertaken currently by the IRI team to establish an IRI-Real-Time (IRI-RT) model by assimilating real-time data into the IRI model [Bilitza *et al.*, 2011]. The reanalysis results can be used for ionospheric weather and climate monitoring and research. It can be improved in the future by using better background models, more accurate estimations of the observation errors and

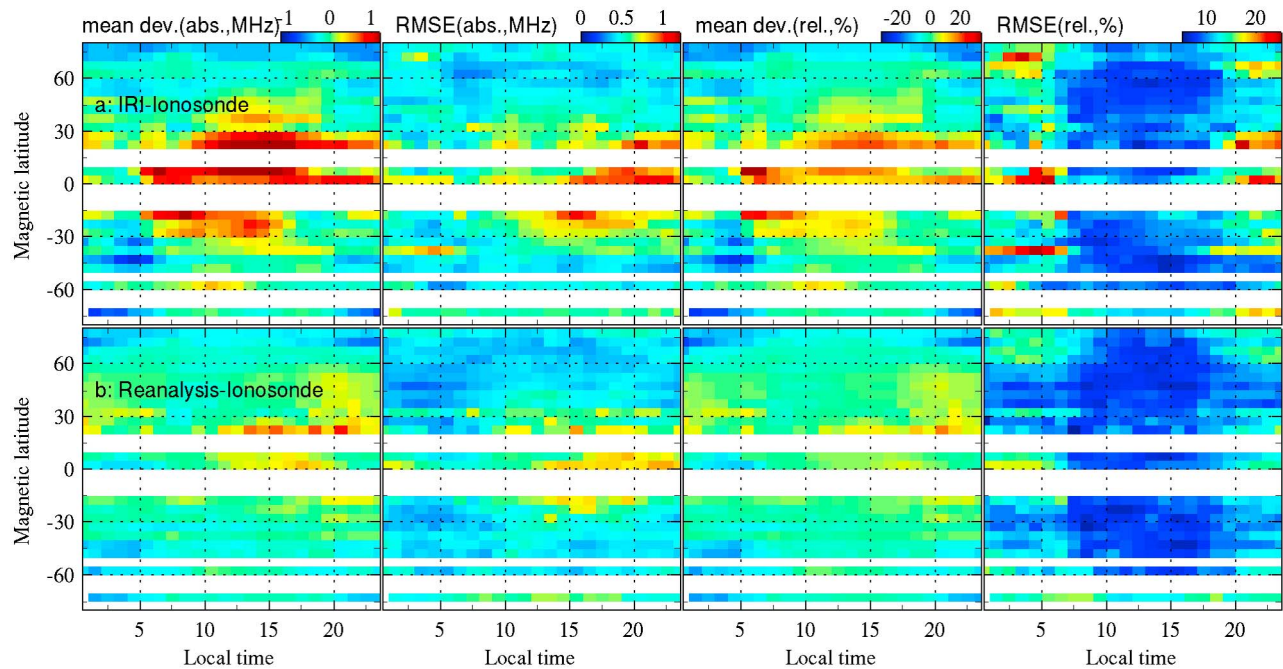


Figure 14. From left to right are shown mean deviation, RMSE of the deviations, mean value of relative deviations, and RMSE of the relative deviations (a) between IRI and ionosonde observations and (b) between reanalysis and ionosonde observations, respectively, during 2007–2011.

ionospheric correlations, and more and diverse data sets that allow for higher spatial and temporal resolutions.

[54] **Acknowledgments.** This material is based upon work supported by the U.S. Air Force with funds awarded via the National Science Foundation under Cooperative Agreement AGS-0918398/CSA AGS-0961147. W. Wang, S. Solomon, and A. Burns are supported by the Center for Integrated Space Weather Modeling (CISM), which is funded by the National Science Foundation's STC program under agreement number ATM-0120950. NCAR is sponsored by the National Science Foundation. W. Wan acknowledges the support from the National Science Foundation of China (41131066, 40904037). The IGS data used in this study includes ground based GNSS observation files, GIM, and GNSS satellites orbits are acquired as part of NASA's Earth Science Data Systems and archived and distributed by the CDDIS (<ftp://cddis.gsfc.nasa.gov>). The global ionosonde data and solar and geomagnetic activity indices are obtained from the SPIDR system at the NOAA/NGDC (<http://ngdc.noaa.gov>). Radar observations by the PFISR are supported by the U.S. National Science Foundation under Cooperative Agreement with SRI International, AGS-1133009, and the data is accessed via the MIT Madrigal database (<http://madrigal.haystack.mit.edu>). We thank GFZ-Potsdam for accessing to the CHAMP, GRACE-A, and TerraSAR-X original data (<http://isdc.gfz-potsdam.de>); JPL/CONAE for the release of the SAC-C original data; and EUMETSAT for providing the Metop-A GRAS original data. Jason-1 and 2 altimeter data were downloaded from NASA/JPL (<ftp://podaac-ftp.jpl.nasa.gov>) and NOAA (<ftp://ftp.nodc.noaa.gov>), respectively.

[55] Robert Lysak thanks the reviewers for their assistance in evaluating this paper.

References

- Afraimovich, E., E. I. Astafyeva, and I. V. Zhivetiev (2006), Solar activity and global electron content, *Dokl. Earth Sci.*, *409*(2), 921–924, doi:10.1134/S1028334X06060195.
- Andreeva, E. S. (1990), Radio tomographic reconstruction of ionization dip in the plasma near the Earth, *J. Exp. Theor. Phys. Lett.*, *52*, 142–148.
- Anthes, R. A. (2011), Exploring Earth's atmosphere with radio occultation: Contributions to weather, climate and space weather, *Atmos. Meas. Tech.*, *4*, 1077–1103, doi:10.5194/amt-4-1077-2011.
- Austen, J. R., S. J. Franke, and C. H. Liu (1988), Ionospheric imaging using computerized tomography, *Radio Sci.*, *23*, 299–307, doi:10.1029/RS023i003p00299.
- Bilitza, D. (2001), International Reference Ionosphere 2000, *Radio Sci.*, *36*(2), 261–275, doi:10.1029/2000RS002432.
- Bilitza, D., and B. W. Reinisch (2008), International Reference Ionosphere 2007: Improvements and new parameters, *Adv. Space Res.*, *42*(4), 599–609, doi:10.1016/j.asr.2007.07.048.
- Bilitza, D., L.-A. McKinnell, B. Reinisch, and T. Fuller-Rowell (2011), The International Reference Ionosphere (IRI) today and in the future, *J. Geod.*, *85*, 909–920, doi:10.1007/s00190-010-0427-x.
- Blewitt, G. (1990), An automatic editing algorithm for GPS data, *Geophys. Res. Lett.*, *17*, 199–202, doi:10.1029/GL017i003p00199.
- Burns, A. G., Z. Zeng, W. Wang, J. Lei, S. C. Solomon, A. D. Richmond, T. L. Killeen, and Y.-H. Kuo (2008), Behavior of the F2 peak ionosphere over the South Pacific at dusk during quiet summer conditions from COSMIC data, *J. Geophys. Res.*, *113*, A12305, doi:10.1029/2008JA013308.
- Bust, G. S., and C. N. Mitchell (2008), History, current state, and future directions of ionospheric imaging, *Rev. Geophys.*, *46*, RG1003, doi:10.1029/2006RG000212.
- Bust, G. S., T. W. Garner, and T. L. Gaussiran II (2004), Ionospheric Data Assimilation Three-Dimensional (IDA3D): A global, multisensor, electron density specification algorithm, *J. Geophys. Res.*, *109*, A11312, doi:10.1029/2003JA010234.
- Dumont, J. P., V. Rosmorduc, N. Picot, S. Desai, H. Bonekamp, J. Figa, J. Lillibridge, and R. Scharro (2009), *OSTM/Jason-2 Products Handbook*, Jet Propul. Lab., Pasadena, Calif.
- Fremouw, E. J., J. A. Secan, and B. M. Howe (1992), Application of stochastic inverse theory to ionospheric tomography, *Radio Sci.*, *27*(5), 721–732, doi:10.1029/92RS00515.
- Gallagher, D. L., P. D. Craven, and R. H. Comford (1988), An empirical model of the Earth's plasmasphere, *Adv. Space Res.*, *8*, 15–24, doi:10.1016/0273-1177(88)90258-X.
- Hajj, G. A., R. Ibanez-Meier, E. R. Kursinski, and L. J. Romans (1994), Imaging the ionosphere with the Global Positioning System, *Int. J. Imaging Syst. Technol.*, *5*, 174–187, doi:10.1002/ima.1850050214.
- Hernández-Pajares, M., J. M. Juan, J. Sanz, R. Orus, A. Garcia-Rigo, J. Feltens, A. Komjathy, S. C. Schaer, and A. Krankowski (2009), The IGS VTEC maps: A reliable source of ionospheric information since 1998, *J. Geod.*, *83*, 263–275, doi:10.1007/s00190-008-0266-1.
- Howe, B. M., K. Runciman, and J. A. Secan (1998), Tomography of the ionosphere: Four-dimensional simulations, *Radio Sci.*, *33*, 109–128, doi:10.1029/97RS02615.
- Imel, D. A. (1994), Evaluation of the TOPEX/POSEIDON dual-frequency ionosphere correction, *J. Geophys. Res.*, *99*(C12), 24,895–24,906.
- Jakowski, N., A. Wehrenpfennig, S. Heise, C. Reigber, H. Lühr, L. Grunwaldt, and T. K. Meehan (2002), GPS radio occultation measurements of the ionosphere from CHAMP: Early results, *Geophys. Res. Lett.*, *29*(10), 1457, doi:10.1029/2001GL014364.
- Kalnay, E., et al. (1996), The NCEP/NCAR 40 year reanalysis project, *Bull. Am. Meteorol. Soc.*, *77*, 437–471, doi:10.1175/1520-0477(1996)077<0437:TNYRP>2.0.CO;2.
- Komjathy, A., L. Sparks, B. D. Wilson, and A. J. Mannucci (2005), Automated daily processing of more than 1000 ground-based GPS receivers for studying intense ionospheric storms, *Radio Sci.*, *40*, RS6006, doi:10.1029/2005RS003279.
- Liu, J. Y., C. Y. Lin, C. H. Lin, H. F. Tsai, S. C. Solomon, Y. Y. Sun, I. T. Lee, W. S. Schreiner, and Y. H. Kuo (2010), Artificial plasma cave in the low-latitude ionosphere results from the radio occultation inversion of the FORMOSAT-3/COSMIC, *J. Geophys. Res.*, *115*, A07319, doi:10.1029/2009JA015079.
- Lühr, H., and C. Xiong (2010), IRI-2007 model overestimates electron density during the 23/24 solar minimum, *Geophys. Res. Lett.*, *37*, L23101, doi:10.1029/2010GL045430.
- Mannucci, A. J., B. D. Wilson, D. N. Yuan, C. H. Ho, U. J. Lindqwister, and T. F. Runge (1998), A global mapping technique for GPS-derived ionospheric total electron content measurements, *Radio Sci.*, *33*(3), 565–582, doi:10.1029/97RS02707.
- Mannucci, A. J., C. O. Ao, X. Pi, and B. A. Iijima (2011), The impact of large scale ionospheric structure on radio occultation retrievals, *Atmos. Meas. Tech. Discuss.*, *4*, 2525–2565, doi:10.5194/amt-4-2525-2011.
- Noll, C. (2010), The Crustal Dynamics Data Information System: A resource to support scientific analysis using space geodesy, *Adv. Space Res.*, *45*(12), 1421–1440, doi:10.1016/j.asr.2010.01.018.
- Pryse, S. E., and L. Kersley (1992), A preliminary experimental test of ionospheric tomography, *J. Atmos. Terr. Phys.*, *54*, 1007–1012, doi:10.1016/0021-9169(92)90067-U.
- Raymund, T. D., J. R. Austen, S. J. Franke, C. H. Liu, J. A. Klobuchar, and J. Stalker (1990), Application of computerized-tomography to the investigation of ionospheric structures, *Radio Sci.*, *25*, 771–789, doi:10.1029/RS025i005p00771.
- Rideout, W., and A. Coster (2006), Automated GPS processing for global total electron content data, *GPS Solut.*, *10*, 219–228, doi:10.1007/s10291-006-0029-5.
- Rocken, C., Y.-H. Kuo, W. Schreiner, D. Hunt, S. Sokolovskiy, and C. McCormick (2000), COSMIC system description, *Terr. Atmos. Oceanic Sci.*, *11*(1), 21–52.
- Schaer, S. (1999), Mapping and predicting the Earth's ionosphere using the Global Positioning System, Ph.D. dissertation, Astron. Inst., Univ. of Bern, Bern.
- Schreiner, W. S., et al. (2011), COSMIC Data Analysis and Archive Center (CDAAC) overview and status, paper presented at 5th FORMOSAT-3/COSMIC Data Users Workshop and ICGPSRO 2011, Nat. Space Org., Taipei, Taiwan.
- Schunk, R. W., et al. (2004), Global Assimilation of Ionospheric Measurements (GAIM), *Radio Sci.*, *39*, RS1S02, doi:10.1029/2002RS002794.
- Sojka, J. J., M. J. Nicolls, C. J. Heinselman, and J. D. Kelly (2009), The PFISR IPY observations of ionospheric climate and weather, *J. Atmos. Sol. Terr. Phys.*, *71*, 771–785, doi:10.1016/j.jastp.2009.01.001.
- Solomon, S. C., T. N. Woods, L. V. Didkovsky, J. T. Emmert, and L. Qian (2010), Anomalous low solar extreme-ultraviolet irradiance and thermospheric density during solar minimum, *Geophys. Res. Lett.*, *37*, L16103, doi:10.1029/2010GL044468.
- Solomon, S. C., L. Qian, L. V. Didkovsky, R. A. Viereck, and T. N. Woods (2011), Causes of low thermospheric density during the 2007–2009 solar minimum, *J. Geophys. Res.*, *116*, A00H07, doi:10.1029/2011JA016508.
- Syndergaard, S. (2000), On the ionosphere calibration in GPS radio occultation measurements, *Radio Sci.*, *35*(3), 865–883, doi:10.1029/1999RS002199.
- Uppala, S., et al. (2005), The ERA-40 re-analysis, *Q. J. R. Meteorol. Soc.*, *131*, 2961–3012, doi:10.1256/qj.04.176.
- Wang, C., G. Hajj, X. Pi, I. G. Rosen, and B. Wilson (2004), Development of the Global Assimilative Ionospheric Model, *Radio Sci.*, *39*, RS1S06, doi:10.1029/2002RS002854.
- Wang, W., T. L. Killeen, A. G. Burns, and R. G. Roble (1999), A high-resolution, three-dimensional, time dependent, nested grid model of the coupled thermosphere-ionosphere, *J. Atmos. Sol. Terr. Phys.*, *61*(5), 385–397, doi:10.1016/S1364-6826(98)00079-0.

- Yue, X., W. Wan, L. Liu, B. Ning, and B. Zhao (2006), Applying artificial neural network to derive long-term foF2 trends in the Asia/Pacific sector from ionosonde observations, *J. Geophys. Res.*, *111*, A10303, doi:10.1029/2005JA011577.
- Yue, X., W. Wan, L. Liu, F. Zheng, J. Lei, B. Zhao, G. Xu, S.-R. Zhang, and J. Zhu (2007a), Data assimilation of incoherent scatter radar observation into a one-dimensional midlatitude ionospheric model by applying ensemble Kalman filter, *Radio Sci.*, *42*, RS6006, doi:10.1029/2007RS003631.
- Yue, X., W. Wan, L. Liu, and T. Mao (2007b), Statistical analysis on spatial correlation of ionospheric day-to-day variability by using GPS and Incoherent Scatter Radar observations, *Ann. Geophys.*, *25*, 1815–1825, doi:10.5194/angeo-25-1815-2007.
- Yue, X., W. S. Schreiner, J. Lei, S. V. Sokolovskiy, C. Rocken, D. C. Hunt, and Y.-H. Kuo (2010), Error analysis of Abel retrieved electron density profiles from radio occultation measurements, *Ann. Geophys.*, *28*, 217–222, doi:10.5194/angeo-28-217-2010.
- Yue, X., W. S. Schreiner, Y.-C. Lin, C. Rocken, Y.-H. Kuo, and B. Zhao (2011a), Data assimilation retrieval of electron density profiles from radio occultation measurements, *J. Geophys. Res.*, *116*, A03317, doi:10.1029/2010JA015980.
- Yue, X., W. S. Schreiner, D. C. Hunt, C. Rocken, and Y.-H. Kuo (2011b), Quantitative evaluation of the low Earth orbit satellite based slant total electron content determination, *Space Weather*, *9*, S09001, doi:10.1029/2011SW000687.
- Yue, X., W. S. Schreiner, C. Rocken, and Y.-H. Kuo (2012a), Validate the IRI2007 model by the COSMIC slant TEC data during the extremely solar minimum of 2008, *Adv. Space Res.*, doi:10.1016/j.asr.2011.08.011, in press.
- Yue, X., W. S. Schreiner, and Y.-H. Kuo (2012b), A feasibility study of the radio occultation electron density retrieval aided by a global ionospheric data assimilation model, *J. Geophys. Res.*, *117*, A08301, doi:10.1029/2011JA017446.